A Study of Hybrid Renewable Energy Production Scenarios Using a Long Short-Term Memory Method. A Case Study of Göksun

Habibe Karayigit[1,*], Aykan Bolukbasi[2], Kadir Abaci[2], Ali Akdagli[2]
[1]*General Directorate of Secondary Education, Ministry of National Education, Adana, Turkiye*
[2]*Department of Electrical-Electronics Engineering, Mersin University, 33110 Mersin, Turkiye*
[*]*habibekarayigit@aof.anadolu.edu.tr; 2002050171015@mersin.edu.tr; kabaci@mersin.edu.tr; akdagli@mersin.edu.tr*

***Abstract*—The global demand for energy has increased exponentially over the years. To reduce the dominance of fossil fuels in energy production, there has been a shift towards energy production models based on renewable sources. In the design of hybrid energy systems, it is essential to keep investment costs low while ensuring the security of the energy supply by meeting the consumer's energy demands without interruption. The success of a good energy production model can be directly associated with the results of load estimation. The primary objective of this research is to predict the electricity demand for the Göksun district until 2028, utilising a data set that encompasses electricity usage from 2019 through the first four months of 2024 for the Göksun district in Kahramanmaraş. This endeavour includes the application of various machine learning (ML) paradigms (long short-term memory (LSTM), gated recurrent unit (GRU), convolutional neural network (CNN)-LSTM, support vector regression (SVR)) to produce load forecasting outcomes and to engineer an optimally performing hybrid system. On evaluation of the performance metrics derived from the experimental data, it has been established that the LSTM model outperforms other methodologies, yielding more favourable results. The simulation studies of the designed hybrid system were conducted using the hybrid optimisation model for electric renewables software (HOMER Pro), demonstrating improvements in both economic and environmental parameters. Our study is unique in that it is the first to utilise a data set specific to the Göksun region and to model predictions obtained from this data set using HOMER software.**

***Index Terms*—LSTM; CNN; GRU; HOMER; Hybrid system; COE; Emission.**

I. INTRODUCTION

The demand for electrical energy is increasing worldwide. Excessive use of fossil resources in electricity production around the world causes serious threats such as global warming, the greenhouse effect, depletion of the ozone layer, and climate changes [1]–[3]. Moreover, the depletion of existing underground resources, deteriorating climate conditions, and negative economic impacts require a greater preference for renewable energy sources over these resources [4].

Manuscript received 3 June, 2024; accepted 28 August, 2024.

However, renewable energy sources exhibit variability according to seasonal conditions. It is not possible to obtain the same amount of energy from various renewable energy sources on every day of the year [5], [6]. On the contrary, it is possible to generate uninterrupted energy regardless of the seasons using energy sources produced using fossil fuels. There should be a balance between these two types of sources for the least expensive production of energy, and they should be integrated into the system accordingly. Power systems that rely solely on a single type of source have now been replaced by hybrid systems that incorporate multiple energy sources. The hybrid optimisation model for electric renewables (HOMER) [7] developed by the National Renewable Energy Laboratory (NREL) is the most used optimisation software for hybrid systems. It is able to optimise hybrid systems consisting of photovoltaic generator, batteries, wind turbines, hydraulic turbines, AC generators, fuel cells, electrolyzers, hydrogen tanks, AC-DC bidirectional converters, and boilers. The loads can be AC, DC, and/or hydrogen loads, as well as thermal loads.

There are numerous studies in the literature regarding the optimisation of grid-connected or standalone hybrid systems. In most of these studies, the HOMER software has been preferred, as it allows for an easier and more precise evaluation of different combinations. Among the studies conducted using HOMER software, Kalamaras, Belekoukia, Lin, Xu, Wang, and Xuan [8] determined that the electricity and thermal needs can be met reliably with a hybrid system on the islands of Greece. Padrón, Avila, Marichal, and Rodríguez [9] examined the technical and economic aspects of hybrid energy system models created in the Canary Islands using the HOMER programme. Tabak [10] used an on-grid hybrid system in the HOMER programme, incorporating a solar power plant, batteries, and a diesel generator to meet the electricity needs of a factory in Konya province. Türkdoğan, Mercan, and Çatal [11] established a hybrid energy system using the HOMER programme to meet the electricity requirements of a farmhouse located in Yalova. The authors in [12] analysed a hybrid photo voltaic (PV)/wind turbine (WT) renewable energy system in Nigeria. They revealed that countries with similar economic and climatic conditions

could benefit from the designed hybrid renewable energy systems (HRES). Duman and Güler [13] utilised HOMER software to perform an economic analysis of grid-connected solar energy systems positioned on rooftops in Turkey. Kılıç and Adalı [14] designed a hybrid wind-solar-grid energy system for a supermarket using the HOMER Pro programme. Shahzad, Zahid, Rashid, Rehan, Ali, and Ahmad [15] performed a sensitivity analysis of biomass potential and cost, amount of solar radiation, and different loads in a rural area of Pakistan. The authors in [16] performed a feasibility analysis of a standalone HRES to find the optimal solution considering the lowest cost of energy (LCOE) and net present cost (NPC). It was observed that the PV/DG/BESS configuration was preferred for microgrid rollout. They have also conducted an analysis of the economic and environmental impacts of renewable energy sources in Ardabil province in Iran [17]. Khan, Yadav, and Mathew [18] demonstrated that the PV-wind-diesel-battery hybrid system is superior to other hybrid systems considered in terms of the unit cost of electrical energy [18]. In addition to these studies, researchers have conducted numerous studies using HOMER software to simultaneously operate energy sources such as solar, wind, and biogas in conjunction with the grid [19]–[25].

With the increasing areas of application of hybrid systems, it is also important how these systems are designed and used. As electricity cannot be stored, it must be generated in the same amount as it will be consumed. Furthermore, due to stochastic and uncertainty characteristics, accurately predicting the future load demand for electrical services has become a challenging problem. Therefore, a good energy production model should offer a solution that aims to maintain the balance between supply and demand, reduce production costs, and manage capacity planning while utilising different sources. The success of a good energy production model can be directly associated with the results of load estimation. When the short- and long-term load demand is accurately estimated, the optimal sizing and effective operation of the hybrid system to be designed are ensured. Load estimation has been an area of great interest for researchers since the past. Apart from the traditional load estimation methods previously used, the use of machine learning and deep learning algorithms has become quite widespread today.

Deep learning technologies continue to play a significant role in forecasting electricity consumption, especially with the increase in studies during the pandemic period. The impact of COVID-19 on electricity consumption was analysed in five states in Germany and the United States using a combination of long short-term memory (LSTM) and autoregressive distributed lag (ARDL) models, revealing a reduction in energy consumption due to the pandemic [26]. In Qatar, econometric time series models and machine learning techniques, including LSTM, were used to predict electricity consumption in various stages of the COVID-19 pandemic, econometric models demonstrating superior performance during the pandemic, while LSTM showed competitive performance in the initial stages [27]. Using a newly collected data set that includes pre and post COVID-19 data, the performance of various machine learning (ML)/deep learning (DL) models (including convolutional neural network (CNN)-gated recurrent unit (GRU)) was evaluated, and the impact of COVID-19 on electricity consumption (EC) models was analysed. The merging customer data and the development of a CNN-GRU model with self-attention features was observed to result in higher prediction accuracy [28]. The newly proposed hybrid support vector regression (SVR) model, tested with American residential electricity consumption data, exhibited superior forecasting accuracy compared to other models such as recurrent neural networks (RNN), generalised regression neural networks (GRNN), and particle swarm optimisation-support vector machine (PSO-SVM), according to experimental results [29].

In this study, load forecasting for the Göksun district was performed using LSTM, GRU, CNN-LSTM, and SVR models with a data set of electricity consumption from 2019 to the first four months of 2024 for the Göksun district in Kahramanmaraş [30]. The LSTM model, which exhibited the best performance (mean absolute error (MAE): 109.70, root mean square error (RMSE): 167.36, mean absolute percentage error (MAPE): 6.01, R-squared (R^2): 0.46), was proposed for a feasible energy production model. Moreover, using the forecast results obtained from the HOMER software, simulation studies of the designed hybrid system aim to reduce economic and environmental parameters while proposing a feasible energy production model intended to meet the demand for electricity in the coming years.

II. Model Design of Using Homer

A. Modelling of the Photovoltaic System

HOMER software performs calculations using specific formulas to determine the energy production from solar energy, which is one of the renewable energy sources utilised in the programme. In the modelling of solar energy panels, the mathematical model that calculates the output power of PV panel arrays is presented as follows

$$P_{PV} = Y_{PV} f_{PV} \left(\frac{G_T}{G_{T,STC}} \right) \left[1 + \alpha_p \left(T_c - T_{c,STC} \right) \right], \qquad (1)$$

where Y_{PV} is the nominal capacity of the PV array in kW, f_{PV} is the derating factor that accounts for losses due to the deviation from the rated power value specified on the DC nameplate, G_T is the solar irradiance (kW/m^2), $G_{T,STC}$ is the irradiance at standard test conditions ($1\ kW/m^2$), α_p is the temperature coefficient of power (%/℃), T_c is the PV cell temperature (℃), and $T_{c,STC}$ is the cell temperature under standard test conditions (℃).

B. Modelling of the Battery System

The maximum battery charging power considered in the battery charge and discharge power calculations performed by the HOMER software is the minimum of three separate limitations on the maximum charging power of the battery bank. In the following equations,

$$\begin{cases} P_{batt,cmax} = \dfrac{MIN\left(P_{batt,cmax,kbm}, P_{batt,cmax,mcr}, P_{batt,cmax,mcc}\right)}{n_{batt,c}}, \\ P_{batt,cmax,kbm} = \dfrac{kQ_1 e^{-k\Delta t} + Qkc\left(1-e^{-k\Delta t}\right)}{1-e^{-k\Delta t} + c\left(k\Delta t - 1 + e^{-k\Delta t}\right)}, \\ P_{batt,cmax,mcr} = \dfrac{\left(1-e^{-\alpha_c \Delta t}\right)\left(Q_{max} - Q\right)}{\Delta t}, \\ P_{batt,cmax,mcc} = \dfrac{N_{Batt}\, I_{max}\, V_{max}}{1000}, \\ n_{batt,c} = \sqrt{n_{batt,rt}}, \\ P_{batt,dmax,kbm} = \dfrac{-kQ_{max} + kQ_1 e^{-k\Delta t} + Qkc\left(1-e^{-k\Delta t}\right)}{1-e^{-k\Delta t} + c\left(k\Delta t - 1 + e^{-k\Delta t}\right)}, \\ n_{batt.d} = n_{batt.c}, \end{cases} \quad (2)$$

where Q_1 is the available energy in the battery at the beginning of the time step (kWh), Q is the total amount of energy in the battery at the beginning of the time step(kWh), Q_{max} is the total storage capacity of the battery (kWh), $c, k\,(h^{-1})$ is the storage capacity ratio, α_c (A/Ah) is the storage rate constant, which is the maximum storage charge rate, Δt is the length of the time step (h), n_{batt} is the number of batteries to be used for storage, I_{max} is the maximum charge current of the batteries (A), V_{nom} is the nominal voltage of the battery (V), $n_{batt,c}$ is the charging efficiency of the battery (%), $n_{batt,rt}$ is the round-trip efficiency, $\mathbf{n_{batt,d}}$ is the maximum discharge power of the battery bank.

C. Inverter

The inverter converts the DC electricity from the PV panels into AC electricity with an efficiency of n_inv, as follows

$$P_{inv,Out} = n_{inv} P_{PV}. \quad (3)$$

D. Examination of the Economic and Environmental Outputs of the Homer Software

One of the most crucial outputs that the HOMER software will ultimately provide among its solutions is the economic analysis. The software presents the most feasible and applicable result to the user for the studied region based on the economic outcomes it generates. The calculation methods used in these results will be explained in this section. Information about the economic terms and calculation methods seen as software results is provided below.

1. Initial Capital Cost (ICC)

ICC is the total cost required for the initial installation of the project with all its components.

2. Net Present Cost (NPC)

NPC provides information about the profitability of a project. The NPC of a project is the value obtained by discounting all future cash flows at the real interest rate. In the NPC method, the present value of all revenues is compared with the present value of all expenses. These cash flow differences provide general information on whether the project is a suitable investment.

Total NPC is the most important economic indicator in HOMER. HOMER ranks systems according to their NPC values. The NPC is calculated using the following formula:

$$\begin{cases} C_{NPC} = \dfrac{C_{yıl,top}}{CRF\left(i, R_{prj}\right)}, \\ CRF\left(i, N\right) = \dfrac{i\left(1+i\right)^N}{\left(1+i\right)^N - 1}, \end{cases} \quad (4)$$

where $C_{yıl,top}$ is the annualised system cost ($/ year), CRF is the capital recovery factor, R_{prj} is the project lifetime, i is the real interest rate, and N is the number of years.

3. Levelized Cost of Energy (COE)

Levelized COE is the ratio of the total cost of a system over its lifetime to the total energy it produces over the same period. To calculate COE, HOMER divides the annualised production cost by the total useful electrical energy production. The expressing COE is as follows

$$COE = \frac{C_{yıl,top}}{E_{AC} + E_{DC} + E_{şeb,s}}, \quad (5)$$

where $C_{yıl,top}$ is the total annualised system cost ($/year), E_{AC} is the amount of AC load served (kWh/year), E_{DC} is the amount of DC load served (kWh/year), $E_{şeb,s}$ is the amount of electricity sold to the grid (kWh/year), $C_{yıl,top}$ is the total annualised cost. $C_{yıl,top}$ is the sum of the annualised costs of all the components of the system and other annualised costs. HOMER uses this value to determine the levelized COE and the total NPC.

4. Calculation of Environmental Impact Using Emission Values

HOMER calculations similarly involve simulation studies where, if a generator is connected to the system, the emissions of environmentally harmful substances such as carbon dioxide in a hybrid system are calculated using the following

$$tCO_2 = 3.667 * m_f * HV_f * CEF_f * X_c, \quad (6)$$

where tCO_2 is the amount of carbon dioxide emissions, m_f is the fuel quantity in liters, HV_f is the fuel heating value (MJ/L), CEF_f is the carbon emission factor (tons of carbon per TJ), and X_c is the oxidized carbon factor.

III. ELECTRICAL LOAD AND LOAD ESTIMATION

The objective of this study is to create models with high accuracy to forecast the electricity consumption of future years from existing data and to develop a feasible energy production model using the forecast results obtained from the HOMER software.

A. Methodology

The data were first subjected to preprocessing, which included date indexing, handling missing values, adding month information, data normalisation, and preparing time series data. Subsequently, four different ML models were applied: LSTM, SVM, CNN-LSTM, and GRU. For each model, training was conducted using the training data, after which the model forecasting capacity was evaluated (Fig. 1).

For the optimisation and analysis of the microgrid,

forecasts for the Göksun region are collected. The cost price for each component is entered into HOMER as an input. A grid search algorithm and a proprietary derivative-free algorithm are used to determine the least costly model. Resources are optimised to maximise usage and keep the cost of electricity production low. The most optimised system architecture is taken as the optimised result. Different costs associated with various components are analysed. Time series data for the entire year are also considered to analyse how the energy balance is achieved by each system component.

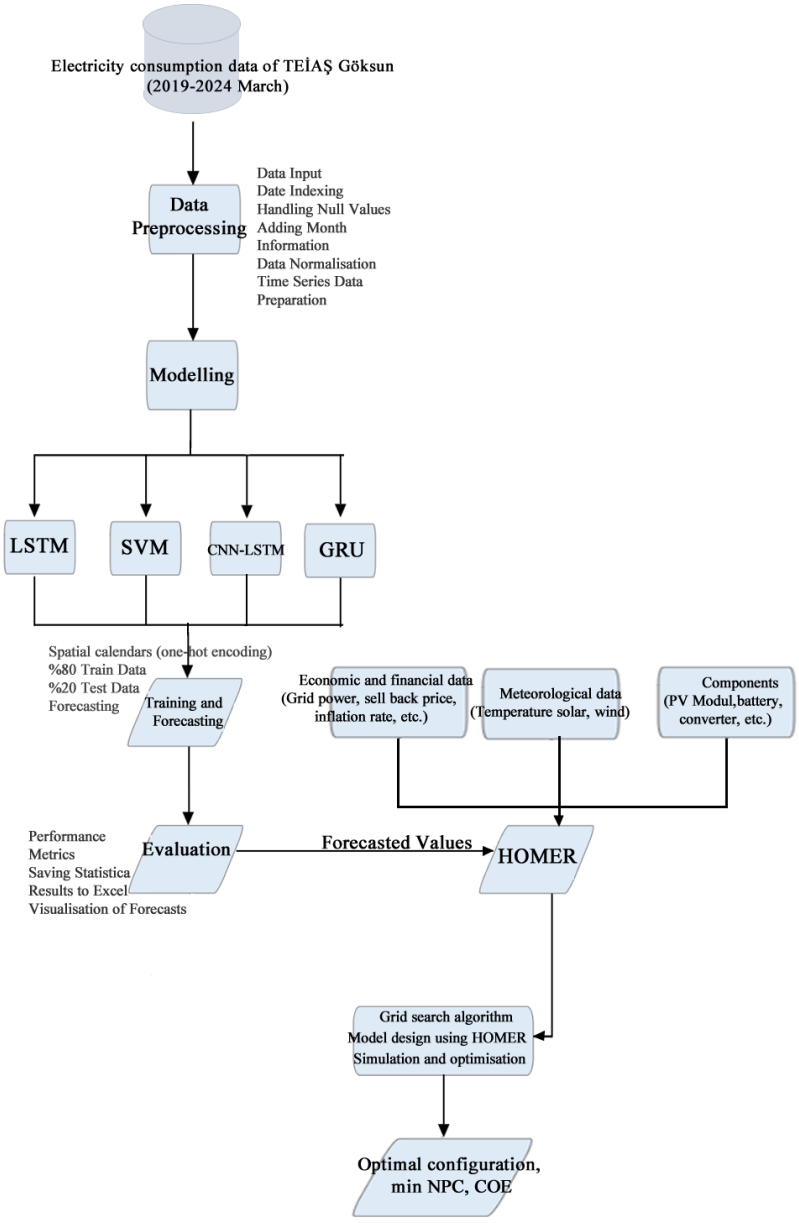

Fig. 1. The overall design of our study.

B. *Research Region (Göksun) and Meteorological Data*

Figure 2 shows the geographical position of Göksun (Lat.: 2 440 N, Long.: 101 420 E, Lat.: 38° 1' 13.3752" North, and Long.: 36° 29' 41.5284" East). The average annual rainfall in the region is 550 ml to 650 ml. The altitude is 1350 meters above sea level. There is an Afşin-Elbistan Thermal central, 40 km from the region, which has an installed capacity of 3.5 MegaWatt (MW). Figure 2 illustrates the location of the Göksun district, its satellite imagery, and the distance between Göksun and the Göksun district that predominantly exhibits a snowy and arid climate throughout most of the year. Winters are characterised by cold temperatures with snowfall, whereas summers experience limited precipitation. Renewable energy resources that can be harnessed in this region include solar, wind, and water sources. Solar radiation data and the corresponding clearness index for the Göksun location, obtained from NASA databases, are illustrated in Fig. 3.

C. *Load Profile and Electrification*

The real load profiles of the Göksun transformer station, obtained from the TEİAŞ Göksun Substation, are provided in Fig. 4 for each month of the year 2023. The decrease in consumption observed in February and March 2023 can be attributed to the earthquake that occurred on February 6, 2023. In this study, the simulation of the system in the HOMER software is performed for 365 days of the year, encompassing a total of 8760 hours.

HOMER synthesises the load profile randomly using the data input for a single day, incorporating stochastic factors. When generating load profiles with the HOMER software,

random variability factors are applied. In Fig. 5, an annual load profile is provided, which is created with a 5 % daily stochasticity and a 5 % stochasticity between time intervals.

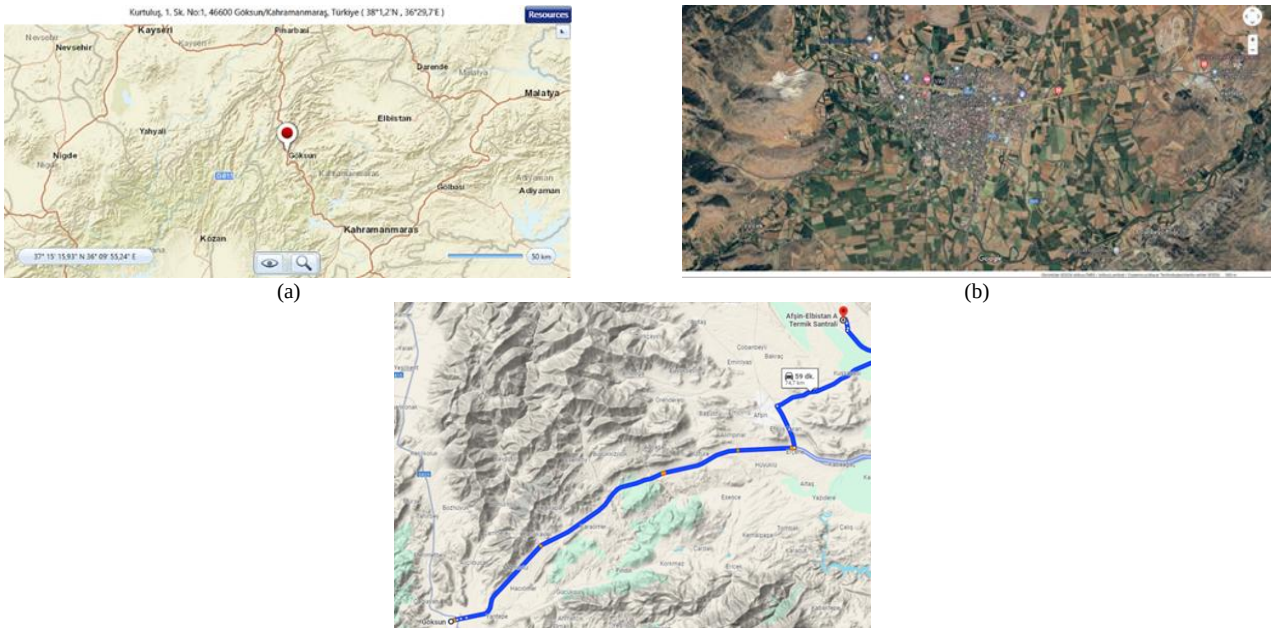

Fig. 2. The research region is Göksun district, specified with (a) its location in Homer and (b) a satellite image from Google Maps (c) its location between Afşin-Elbistan Thermal power plant and Göksun.

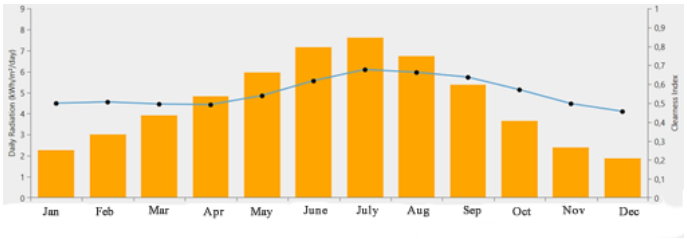

Fig. 3. Graph of solar radiation data and the clearness index, depicting the fluctuations of both variables over time and their influence on the availability of solar energy.

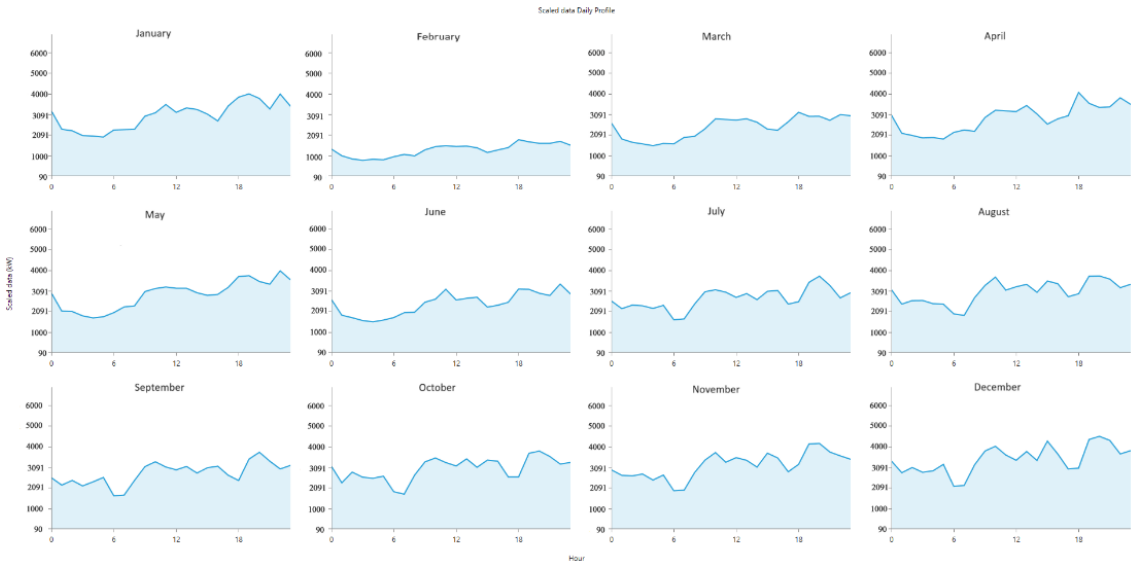

Fig. 4. Monthly average load data for the year (HOMER).

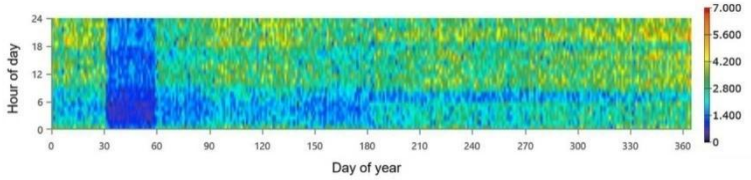

Fig. 5. Annual load profile generated by HOMER showing the change in electrical energy demand.

D. Time Series Models

A time series is a sequence of data points observed over specific time intervals. The LSTM algorithm, which aims to address the gradient issues encountered in RNN methods through the use of forget and output gates, is a prevalent deep learning model in time series analysis [31].

The fundamental components of LSTM consist of the input gate (i_t), forget gate (f_t), and output gate (o_t). The forget gate ascertains the information that ought to be forgotten in the memory by examining the current input (x_t) and the previous state information (h_{t-1}). The input, forget, and output gates serve as components that regulate the updating status of the hidden state information (h_t) and memory cells (c_t) (Fig. 6).

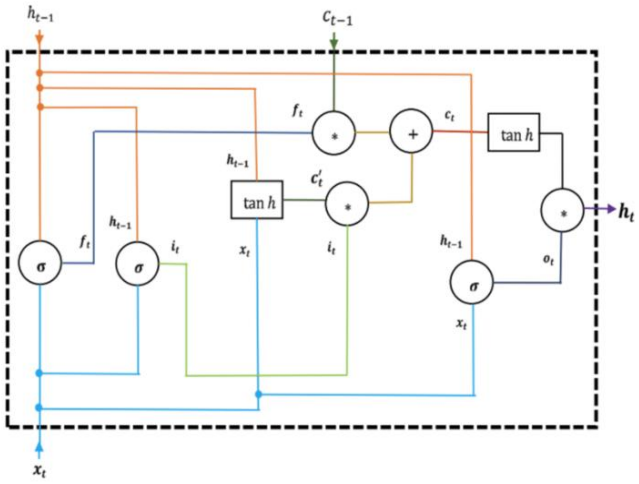

Fig. 6. Architecture of the LSTM algorithm showing the basic components such as input layer, forget gate, input gate, cell state, output gate, and output layer [32].

In Fig. 6, the candidate memory cell, denoted as ($c_t^{'}$), is being designed. Since the actions of the various gates have not yet been determined, the candidate memory cell $c_t^{'}$is introduced for the first time. To compute the value of the candidate memory cell $c_t^{'}$, a tanh activation function is used, similar to those employed by the three gates presented above. The equation corresponding to time step t for $c_t^{'}$ is calculated as shown in the formulas table, where $w_f$represents the memory cell weight value, and c is the bias parameter.

In an LSTM model, there are two special gates that manage the inputs and forgetting. The amount of new data added, denoted as ($c_t^{'}$), is controlled by (i_t). The second gate, which is the forget gate, f_t, indicates how much of the previous content of the memory cell, (c_{t-1}), still remains. Consequently, the update equation for (c_t) is determined as follows:

$$\begin{cases} i_t = \sigma\left(w_i.\left[h_{t-1}, x_t\right] + b_i\right), \\ f_t = \sigma\left(w_f.\left[h_{t-1}, x_t\right] + b_f\right), \\ o_t = \sigma\left(w_o.\left[h_{t-1}, x_t\right] + b_o\right), \\ c_t^{'} = tanh\left(w_c.\left[h_{t-1}, x_t\right] + c\right), \\ c_t = f_t.c_{t-1} + i_t * c_t^{'}, \\ h_t = o_t * tanh\left(c_t\right), \end{cases} \quad (7)$$

where w_i is the input gate weight value, w_f is the forget gate weight value, w_o is the output gate weight value, w_c is the memory cell weight value, σ is the sigmoid activation function, b is the bias value, o_t is the node output value at time t, $c_t^{'}$ is the candidate cell state at time t, calculated using the hyperbolic tangent activation function to create a new memory content based on the previous hidden state and the current input, c_t is the current cell state at time t, which is updated by combining the previous cell state c_{t-1} with the input gate i_t and the forget gate f_t, h_t is the hidden state output at time t, which is derived from the current cell state c_t and the output gate o_t using the hyperbolic tangent activation function.

GRU is also a variant of RNN and is designed to capture long-term dependencies. GRU cells regulate the flow of information using memory cells and gate mechanisms. In sequence prediction tasks, GRU cells are connected in succession, and at each step, a prediction is generated. Each GRU cell receives the previous hidden state (h_{t-1}) and the current input (x_t), computes the update and reset gates, forms the candidate hidden state, and updates the final hidden state. The last hidden state (h_t) is then fed into an output layer to produce the prediction value. During training, the GRU network optimises its parameters (weights and biases) using a loss function that minimises the discrepancy between the actual values and the predicted values.

CNN, renowned for its superior performance in visual data analysis, can also yield impressive results in the prediction of time series data. CNN employ filters to learn patterns from time series data. These filters analyse specific segments of the time series data and extract features.

In our study, the used CNN-LSTM model initially extracts local features from time series data using a Conv1D layer. Subsequently, the LSTM layer learns long-term dependencies using these features. Finally, a dense layer generates the prediction using the hidden state of the LSTM layer.

To facilitate comparison, four popular algorithms have been implemented: SVR [33], GRU [34], a CNN-LSTM hybrid model, and the LSTM model [35].

Parameters for the prediction models were optimised using a trial-and-error approach and were configured as follows: 1) SVR, a variant of SVM was used with the “rbf” kernel function. The penalty parameter C and epsilon were set to 10 and 0.1, respectively. 2) The CNN-LSTM model used includes a Conv1D layer to capture local features in time series data and an LSTM layer to capture long-term dependencies. The first layer is a Conv1D layer with 64 filters and a kernel size of 2, while the second layer is an LSTM layer with 50 units. The model incorporates a dropout (0.2) layer to avoid overfitting. 3) The GRU model consists of two GRU layers to capture dependencies in time series data, along with Dropout layers and an L2 regulariser to mitigate overfitting. The first GRU layer has 200 units with return_sequences=True, while the second GRU layer has 100 units and returns the final cell state. (4) The proposed LSTM model comprises three LSTM layers to capture long-term dependencies in time series data. The first two layers are configured with return_sequences=True, allowing the outputs to be returned as sequences, while the third layer, with return_sequences=False, returns the final cell state. The LSTM model layers utilise 512, 512 and 256 units with a “relu” activation function, in addition to dropout layers and an L2 regulariser.

E. Evaluation Criterion

The following MAE, RMSE, MAPE, and R2 metrics were used to evaluate the prediction performance of the ML models:

$$\begin{cases} MAE = \frac{1}{n}\sum_{i=1}^{n}|y_i - \hat{y}_i|, \\ RMSE = \sqrt{\frac{1}{n}\sum_{i=1}^{n}(y_i - \hat{y}_i)^2}, \\ MAPE = \frac{1}{n}\sum_{i=1}^{n}\left|\frac{y_i - \hat{y}_i}{y_i}\right| * 100, \\ \mathrm{R}^2 = 1 - \frac{\sum_{i=1}^{n}(y_i - \hat{y}_i)^2}{\sum_{i=1}^{n}(\bar{y}_i - y_i)^2}, \end{cases} \quad (8)$$

where n is for the sample size, $\hat{y}_i$ is for the prediction, $\bar{y}_i$ is for the average value, and y_i is for the observation.

IV. Forecasting and Simulation

A. Forecasting Comparisons

In this section, the prediction results of seven prediction models have been compared with the comparison metrics, and the graph of these comparison results has been provided.

Figure 7 shows the real data of electricity consumption along with various predictions of the ML model from 2019 to 2024. The metric mean squared error (MSE) has been used to measure the accuracy performance of the predictions. MSE evaluates the prediction accuracy of the model by taking the average of the squares of the differences between the predicted values and the actual values. A lower MSE value indicates that prediction of the model is closer to the actual data. The LSTM model has performed well in accurately predicting high-consumption periods in 2020 and 2021. The GRU model, on the other hand, was more successful in predicting low-consumption periods in 2022 and 2023. The CNN-LSTM model has generally performed well to follow the actual data. The SVR model was the most successful model in predicting high-consumption periods in 2021 and 2022. However, there were deviations in some periods. The February 2023 period is where the difference between the predictions of the models and the actual consumption value is the highest. This significant deviation is due to the earthquake that occurred in Turkey on 6 February 2024. Extraordinary circumstances, such as earthquakes, can cause sudden drops in electricity consumption.

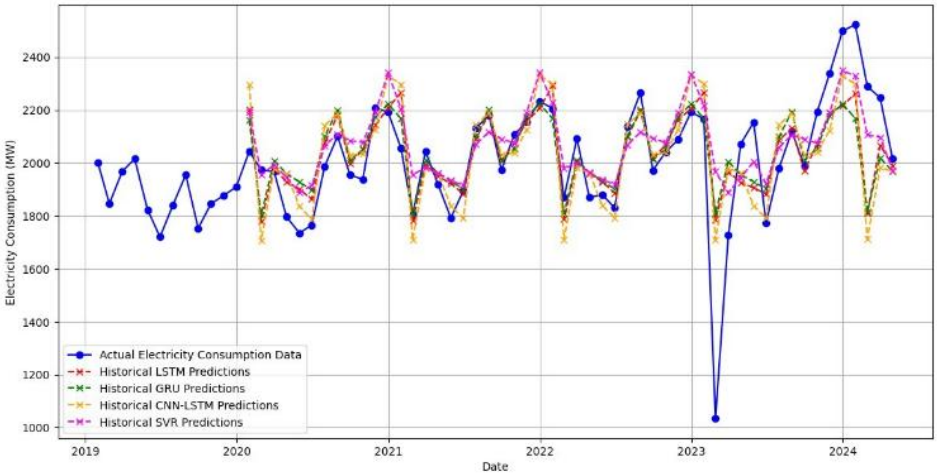

Fig. 7. Actual electricity consumption data and model predictions over the years 2019–2024.

According to the data obtained in Table I, when predicting the original demand series, the SVR model has an MAE of 115.01, an RMSE of 170.24, an MAPE of 6.52 %, and an R^2 value of 0.44. The GRU model has an MAE of 112.61, an RMSE of 172.94, a MAPE of 6.19 %, and an R^2 value of 0.42. The CNN-LSTM model has an MAE of 127.11, an RMSE of 179.56, an MAPE of 6.75 %, and an R^2 value of 0.37. The LSTM model, on the other hand, has an MAE of 109.70, an RMSE of 167.36, a MAPE of 6.01 %, and an R^2 value of 0.46.

These results indicate that the LSTM model performs better than other models in predicting the original demand series, while the SVR and GRU models show similar performance, and the CNN-LSTM model shows a lower performance compared to other models. Particularly, the LSTM model has the lowest MAE, RMSE, and MAPE values, and also has the highest R^2 value. This demonstrates that the LSTM model makes the most accurate predictions when estimating the original demand series.

In all the prediction model graphs obtained in Fig. 8, it is observed that the electricity demand increases as the years progress (from 2023 to 2028). This indicates that energy demand will continue to increase in the future. Additionally, seasonal fluctuations are observed in all models in Fig. 8. Particularly, the electricity demand is higher during the summer months (June, July, August). This is likely related to the increased cooling requirements.

TABLE I. THE FORECASTING PERFORMANCE OF ALL BENCHMARK MODELS.

Model	Forecasting original demand			
	MAE	RMSE	MAPE (%)	R^2
SVR	115.01	170.24	6.52	0.44
GRU	112.61	172.94	6.19	0.42
CNN-LSTM	127.11	179.56	6.75	0.37
LSTM	109.70	167.36	6.01	0.46

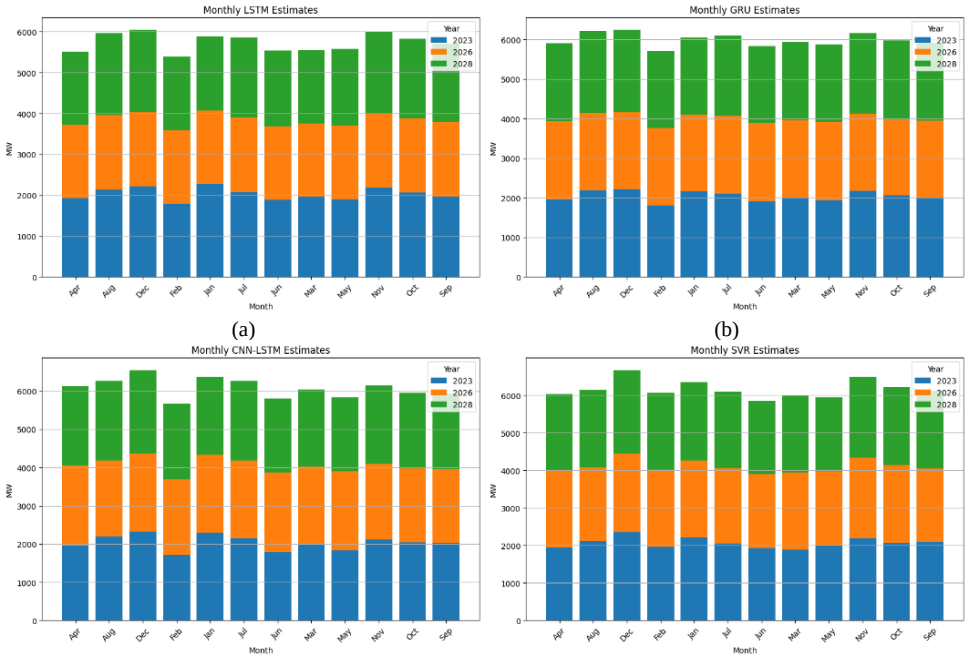

Fig. 8. (a) Monthly LSTM estimates; (b) Monthly GRU estimates; (c) Monthly CNN-LSTM estimates; (d) Monthly SVR estimates.

Furthermore, when examining the energy consumption forecasts for future years in Fig. 8 on a model basis, the predictions of the LSTM model appear more stable compared to other models and show significantly higher estimates for 2028. The predictions of the GRU model follow a trend similar to that of LSTM, but forecast higher values in some months, particularly during the summer. Pronounced fluctuations are observed especially in the summer and winter months. The energy consumption predictions of the CNN-LSTM model for future years exhibit a higher variance compared to the LSTM and GRU models. It has particularly made higher predictions than other models during the month of August. The predictions of the SVR model demonstrate more pronounced seasonal fluctuations, and it has made relatively lower predictions for some months, especially during the winter months.

B. Configuration of the Model System and Component Data

Turkey aims to increase its solar energy capacity by around 500 % to reach 52.9 gigawatts by 2035, making solar energy the source with the highest installed capacity [36]. This study focusses on the techno-economic and environmental analysis of the region, using the LSTM model and the load forecast values for 2026 and 2028. The current photovoltaic production of Göksun district is projected to increase from 4.82 MW to 8000 MW in 2026 and 10000 MW in 2028. This study focusses on the optimal hybrid design for 2026 and 2028 using the load predictions obtained through the LSTM model, as it gives better results in predictive modelling. Throughout the simulation, assuming inflation expectations of 0 %, 4 %, and 8 %, potential price increases have been uniformly applied to all components of the system except the PV modules. Anticipating that PV production technology will advance rapidly and production costs will decrease over the years, a 10 % reduction has been applied to the capital and replacement costs of the PV system. Changes in inflation rates have been similarly reflected in grid power prices and sellback values.

In this section, an evaluation of the technical, economic, and environmental performance of a PV hybrid system is carried out in the Göksun district based on the current situation and the results of the load forecast for 2026 and 2028. Various scenarios have been proposed for the analysis of optimal system performance, and the results are presented in comparative tables.

Figure 9 illustrates a simplified schematic diagram of the grid-connected (hybrid) system. Detailed information on the PV panels, converter, and battery used in the designed system is provided below.

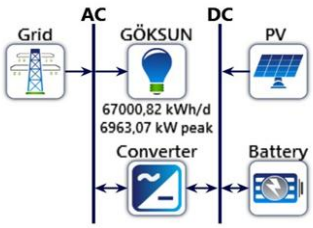

Fig. 9. General configuration of a hybrid electricity generation system including a photovoltaic system, battery storage, and grid connection.

1. PV Modul

The standard test conditions (STC) for the PV panel to be used in simulations in the HOMER programme are considered to be irradiance of 1000 W/m^2, cell temperature of 25 °C, and measurement tolerance of ±3 %.

2. Converter

In the study, the Huawei-45KTL model inverter, which is capable of producing a pure sine wave, has been selected.

3. Battery

The designed hybrid system will use a BAE brand 210 Ah maximum capacity battery. BAE PVS Block solar batteries require minimal maintenance and are used to store electrical energy in solar power plants. The BAE PVS 210 Ah 12 V

model has a dry weight of 51 kilogrammes. Its dimensions are 380 mm in length, 205 mm in width, and 385 mm in height. More detailed technical specifications for the PV module converter and battery, as well as investment cost information, are provided in Appendix A, Table A-I.

– Case 1. Base System.

In the first case, the Göksun district was examined according to the available resources. The schematic representation of the hybrid system designed in the HOMER programme to reflect the current situation is shown in Fig. 9. The cost of electricity sold by the grid is set at $0.099 kWh, with an annual inflation rate of 4 % and a project lifespan of 25 years. The load demand has been met by both renewable sources and the grid. For this case, the optimal values of all system components were determined, resulting in the lowest COE of $0.0792 and the lowest NPC of $85.9 million, with an operating cost of $1.92 million. The optimal number of batteries is 166, and the optimal converter capacity is 4007 kW. Figure 10, which shows the average monthly electricity generation, indicates that the annual PV production is 7149.013 kWh. Figure 11 clearly demonstrates that as PV production and converter utilisation capacity increase, the amount of CO_2 emissions decreases from 15458.85 kg/year to 11387.46 kg/year.

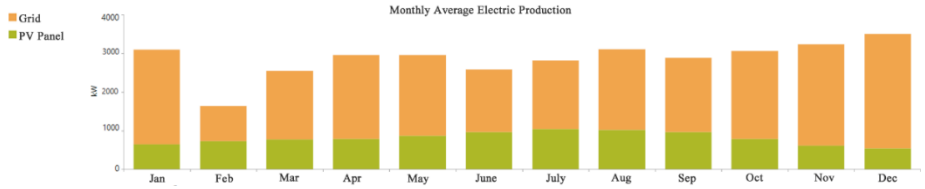

Fig. 10. Monthly actual consumption data for 2023.

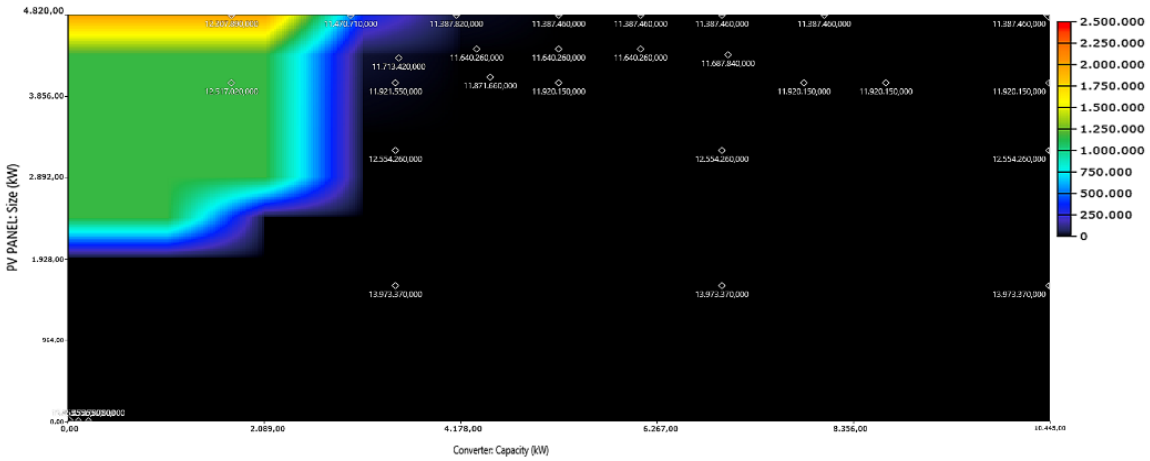

Fig. 11. Correlation between annual electricity production and CO_2 emissions.

– Case 2. The Hybrid System Designed for the Year 2026.

Figure 9 presents the schematic representation of the hybrid system for the year 2026. The forecasted load demand for the year 2026 has been calculated as 82037.06 kWh/d. This section examines the three scenarios. In the first scenario, the installed PV capacity in the region remains constant at the power level of 2023 until 2026. In the second and third scenarios, it increases to 6 MW and 8 MW, respectively. In these scenarios, the economic and environmental impacts, considering the effect of inflation, will be discussed. In this case study, the design of an 8 MW solar power plant is the most favourable scenario in terms of economic and environmental parameters. In this scenario, as the PV production and converter usage capacity increases, the amount of CO_2 emissions decreases from 11545.576 kg/year to 10178.873 kg/year. This amount has been obtained in the black-coloured region where the excess electricity is the lowest. It is evident that the increase in inflation negatively affects the economic parameters. Other system data for all three scenarios for the year 2026 are provided in Table II.

– Case 3. The Hybrid System Designed for the Year 2028.

Figure 12 shows the schematic representation of the hybrid system for the year 2028. The load forecast for this year, estimated using the LSTM model, has been calculated as 87068.93 kWh/d. This case study presents PV production forecasts for the year 2028 under three different scenarios. In the first scenario, the level of PV production is assumed to remain constant at 4.82 MW, the same as in 2023.

In the second scenario, PV production is projected to reach the highest expected level of 8 MW by 2026. For the final scenario, PV production is expected to increase to 10 MW by 2028. Table II presents the results obtained for this case study. The increase in PV production has had positive impacts, resulting in reductions in both economic and environmental parameters.

The increase in the number of batteries and converter capacity has also contributed to the reduction of these parameters. Figure 13 illustrates the reduction in CO_2 emissions from 20082.0 kg/year to 13416.83 kg/year, demonstrating the impact of increased PV production and converter usage capacity. Examining the scale values of the surface colours in the figure clearly shows that the amount of excess electricity increases as PV production increases.

Figure 14 is plotted to show how COE is affected for the years 2026 and 2028 in the planned hybrid system under inflation expectations of 0 %, 4 %, and 8 %. This graph demonstrates that increasing PV production yields positive results in environments with low inflation.

TABLE II. ECONOMIC AND ENVIRONMENTAL PARAMETERS OF THE HYBRID SYSTEM DESIGNED FOR THE YEARS 2023, 2026, AND 2028.

Parameters	Case I	Case II			Case III		
	Base system	Scenario 1	Scenario 2	Scenario 3	Scenario 1	Scenario 2	Scenario 3
COE ($)	0.0791	0.0887	0.08129	0.0689	0.0949	0.08568	0.07522
NPC ($) *$10^6$	8.586	9.585	9.075	8.300	10.29	12.55	11.66
Battery	116	200	11	268	69	55	150
Ren. Fraction (%)	28.1	28.2	33.9	42	28.1	34.5	40.7
Excess electricity (%)	0.064	0.062	0.065	0.025	0.0317	0.0289	0.0708
Converter (kW)	4007	4019	5039	7088	4160	6574	8449
CO_2 [kg/year]	11388.324	11329.156	10760.846	10178.873	11377.427	14000.293	13416.829
SO_2 [kg/year]	49374	49117.0	46.653	44.130	49.326	60.697	58.168
NOx [kg/year]	24146	24021.0	22.816	21.582	24.123	29.684	28.447

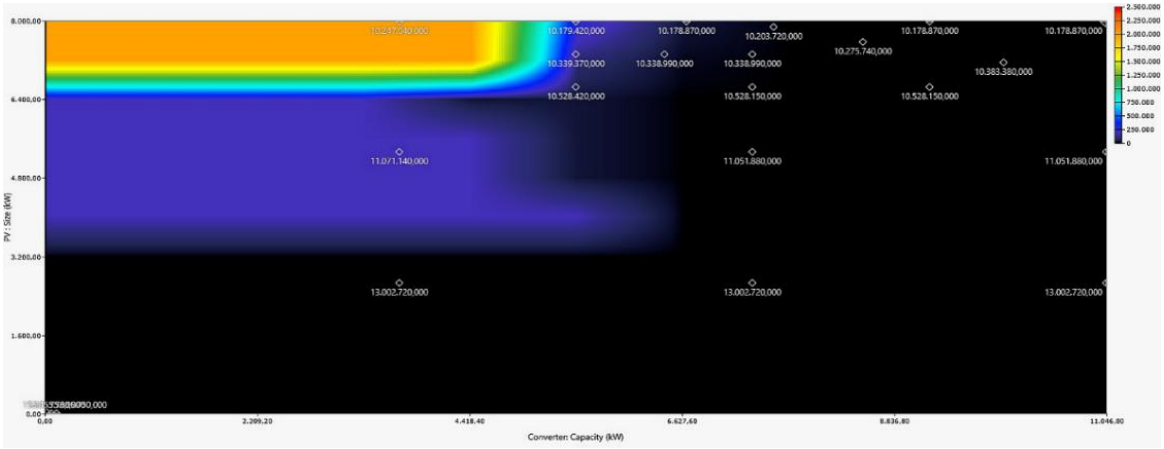

Fig. 12. Correlation between annual electricity production and CO_2 emissions.

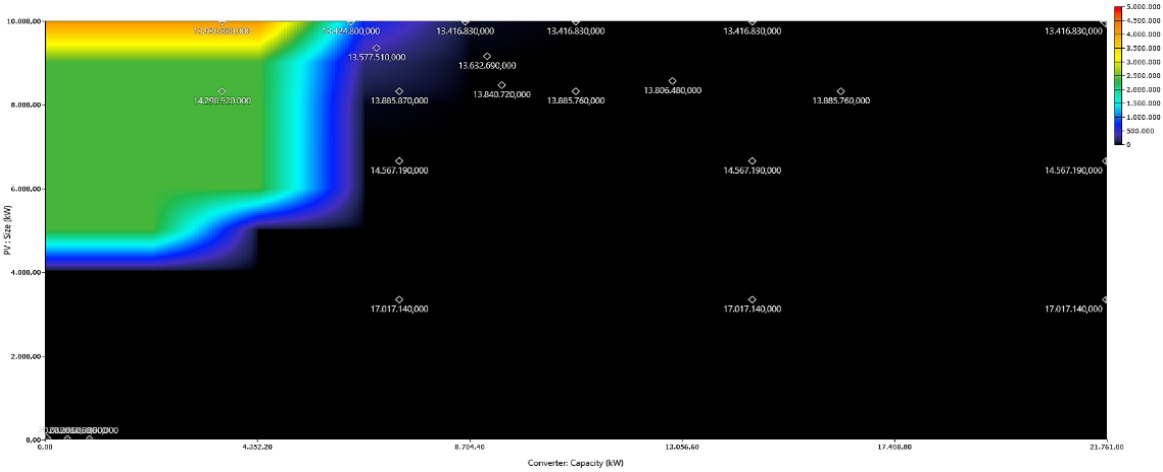

Fig. 13. Correlation between annual electricity production and CO2 emissions.

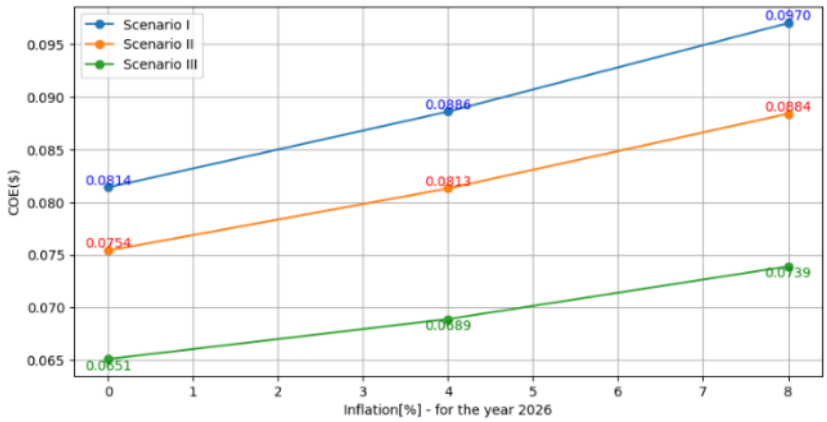

(a)

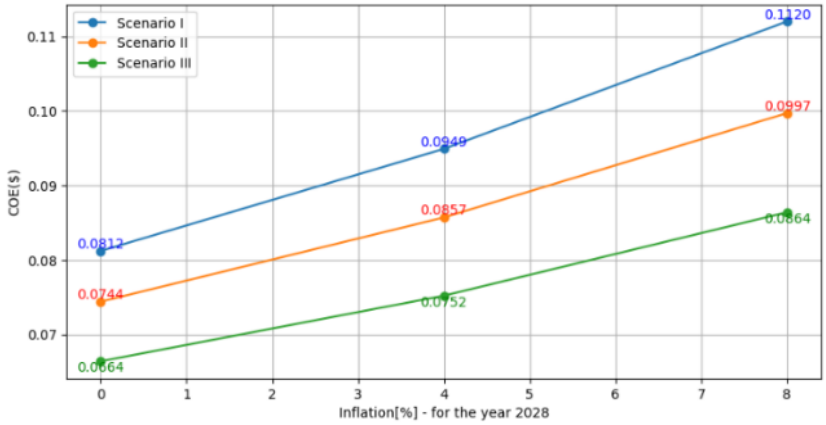

(b)

Fig. 14. Impact of inflation on the COE: (a) 2026 year; (b) 2028 year.

V. DISCUSSIONS

The increase in energy demand and the inability to store electricity make forecasting the future load requirements of a region a challenging problem. A well-designed load forecasting model should not only reduce the cost of the system being designed but also maintain the balance between supply and demand.

In this study, several ML models, namely LSTM, GRU, CNN-LSTM, and SVR were used to forecast electricity consumption in the Göksun district of the Kahramanmaraş province for the period 2019–2024. The LSTM model excelled in accuracy compared to other models and successfully captured the high-consumption periods in 2020 and 2021. The SVR model also achieved close results to LSTM, accurately predicting elevated consumption levels in 2021–2022. Meanwhile, the GRU model performed well during low-consumption periods, while the CNN-LSTM model generally followed the trend but was less successful than the other models. The earthquake that occurred in Turkey in February 2023 created the largest discrepancy between the prediction of the model and the actual consumption, highlighting the impact of such unforeseen events on electricity use and the need for models to account for them.

In this study, the LSTM model performed the best, but the optimal model may vary depending on different data sets and applications. Therefore, it is essential to compare the performance of various models to determine the most suitable one. The data set used in this research is relatively small; larger data sets spanning longer time frames could enhance the accuracy of the models. Electricity consumption is impacted by a multitude of external factors, including economic expansion, population growth, climatic conditions, and unforeseen events. Enhancing the accuracy of the models could be achieved by integrating these factors. The prediction results obtained from this study can serve as a valuable input in designing a hybrid energy system that is tailored to the needs of the Göksun district. Demand forecasts generated using the LSTM model can help optimising the integration of renewable energy sources such as solar and wind power and determining the appropriate dimensions of energy storage systems. In conclusion, among the compared models, the LSTM model has been observed to be effective in capturing the underlying trends and variations in load data, making significant contributions to the design of hybrid systems. However, the impact of extraordinary situations and the need to consider additional variables stand out as crucial research areas for future studies. In this context, the design of hybrid models and continuous updates will play a critical role in improving the accuracy of electricity consumption forecasts.

VI. CONCLUSIONS

The results have shown that increasing the current photovoltaic energy production of 4.82 MW in the Göksun district would yield positive results in terms of economic and environmental parameters. Despite the projected increase in load demand for the years 2026 and 2028, the designed system scenarios have reduced the current COE from $0.079 to $0.0689, and $0.075, respectively. Furthermore, the amount of CO^2 emissions released into the environment has decreased from 20082.0 kg/year to 13416.83 kg/year in response to the increasing load demand.

APPENDIX A

TABLE A-I. TECHNICAL SPECIFICATIONS AND ECONOMIC PARAMETERS OF SYSTEM COMPONENTS.

Component	Specification	Value	Capital Cost ($)	Replacement ($)	O&M ($/year)
	Maximum Power (Wp)	500			
	Voltage at Maximum Power (V)	38,46			
	Current at Maximum Power (A)	13,01			
PV (1 kW)	Open-Circuit Voltage (V) Short Circuit Current (A)	45,52 13,80	125	125	10
	Efficiency	%20,9			
	Max. voltage (DC V)	1500			
	Cell Operating Temperature (°C)	45 ±2			
	Maximum Input Voltage (V)	1500			
	Maximum Input Current (A)	22			
	Maximum Short-Circuit Current (A)	30			
Converter (45 kW)	Output Power (W)	45000	3500	3500	100

Component	Specification	Value	Capital Cost ($)	Replacement ($)	O&M ($/year)
	Maximum Apparent Power (VA)	50000			
	Maximum Capacity (Ah)	210			
1 Battery	Operating Voltage (V)	12	315	300	-
	Weight (kg)	51			

CONFLICTS OF INTEREST

The authors declare that they have no conflicts of interest.

REFERENCES

[1] A. H. Eisapour, M. Eisapour, M. J. Hosseini, A. H. Shafaghat, P. Talebizadeh Sardari, and A. A. Ranjbar, "Toward a highly efficient photovoltaic thermal module: Energy and exergy analysis", *Renewable Energy*, vol. 169, pp. 1351–1372, 2021. DOI: 10.1016/j.renene.2021.01.110.

[2] N. Apergis and J. E. Payne, "Energy consumption and economic growth: Evidence from the Commonwealth of Independent States", *Energy Economics*, vol. 31, no. 5, pp. 641–647, 2009. DOI: 10.1016/j.eneco.2009.01.011.

[3] "World Carbon Dioxide Emissions: 1950-2050", JSTOR. [Online]. Available: https://www.jstor.org/stable/2646725

[4] R. Alayi, M. H. Ahmadi, A. R. Visei, S. Sharma, and A. Najafi, "Technical and environmental analysis of photovoltaic and solar water heater cogeneration system: A case study of Saveh City", *International Journal of Low-Carbon Technologies*, vol. 16, no. 2, pp. 447–453, 2021. DOI: 10.1093/ijlct/ctaa077.

[5] A. Agga, A. Abbou, M. Labbadi, Y. El Houm, and I. H. Ou Ali, "CNN-LSTM: An efficient hybrid deep learning architecture for predicting short-term photovoltaic power production", *Electric Power Systems Research*, vol. 208, art. 107908, 2022. DOI: 10.1016/j.epsr.2022.107908.

[6] H. Kumbur, Z. Özer, H. D. Özsoy, and E. D. Avcı, "Türkiye'de geleneksel ve yenilenebilir enerji kaynaklarının potansiyeli ve çevresel etkilerinin karşılaştırılması", in *Proc. of 3rd Renewable Energy Resources Symposium and Exhibition*, 2005, pp. 19–21. [Online]. Available: https://www.emo.org.tr/ekler/3f445b0ff5a783e_ek.pdf

[7] "HOMER (The Hybrid Optimization Model for Electric Renewables)", 2024. [Online]. Available: http://www.nrel/gov/HOMER

[8] E. Kalamaras, M. Belekoukia, Z. Lin, B. Xu, H. Wang, and J. Xuan, "Techno-economic assessment of a hybrid off-grid DC system for combined heat and power generation in remote islands", *Energy Procedia*, vol. 158, pp. 6315–6320, 2019. DOI: 10.1016/j.egypro.2019.01.406.

[9] I. Padrón, D. Avila, G. N. Marichal, and J. A. Rodríguez, "Assessment of Hybrid Renewable Energy Systems to supplied energy to Autonomous Desalination Systems in two islands of the Canary Archipelago", *Renewable and Sustainable Energy Reviews*, vol. 101, pp. 221–230, 2019. DOI: 10.1016/j.rser.2018.11.009.

[10] A. Tabak, "Analysis and design of a hybrid energy generation system to meet the energy demand of a factory in the City of Konya", *International Journal of Engineering Research and Development*, vol. 13, no. 1, pp. 220–230, 2021. DOI: 10.29137/umagd.794898.

[11] S. Türkdoğan, T. Mercan, and T. Çatal, "Meeting the electrical and thermal load requirements of a 40-household community using off-grid hybrid energy systems: Technical and economic analyses", *European Journal of Science and Technology*, no. 18, pp. 476–485, 2020. DOI: 10.31590/ejosat.688048.

[12] E. C. Obuah, C. O. Ahiakwo, E. U. Okowa, and E. J. Diema, "Analysis of autonomous hybrid wind/photovoltaic renewable energy system with load variation", *International Research Journal of Innovations in Engineering and Technology*, vol. 4, no. 2, pp. 44–51, 2020.

[13] A. C. Duman and Ö. Güler, "Economic analysis of grid-connected residential rooftop PV systems in Turkey", *Renewable Energy*, vol. 148, pp. 697–711, 2020. DOI: 10.1016/j.renene.2019.10.157.

[14] M. Y. Kılıç and S. Adalı, "Hybrid renewable energy system for meeting electricity demand - The case of a supermarket", *Osmaniye Korkut Ata University Journal of the Institute of Science and Technology*, vol. 5, no. 1, pp. 224–235, 2022. DOI: 10.47495/okufbed.998900.

[15] M. K. Shahzad, A. Zahid, T. ur Rashid, M. A. Rehan, M. Ali, and M. Ahmad, "Techno-economic feasibility analysis of a solar-biomass off grid system for the electrification of remote rural areas in Pakistan using HOMER software", *Renewable Energy*, vol. 106, pp. 264–273, 2017. DOI: 10.1016/j.renene.2017.01.033.

[16] A. Amupolo, S. Nambundunga, D. S. P. Chowdhury, and G. Grün, "Techno-economic feasibility of off-grid renewable energy electrification schemes: A case study of an informal settlement in Namibia", *Energies*, vol. 15, no. 12, p. 4235, 2022. DOI: 10.3390/en15124235.

[17] S. O. Mohammadi-Aylar, M. Almassi, and H. Bakhoda, "Economic, environmental and energy analysis of the utilization of renewable energy based on Analytic Hierarchy Process: A case study", *International Journal of Low-Carbon Technologies*, vol. 17, pp. 430–435, 2022. DOI: 10.1093/ijlct/ctac017.

[18] M. J. Khan, A. K. Yadav, and L. Mathew, "Techno economic feasibility analysis of different combinations of PV-Wind-Diesel-Battery hybrid system for telecommunication applications in different cities of Punjab, India", *Renewable and Sustainable Energy Reviews*, vol. 76, pp. 577–607, 2017. DOI: 10.1016/j.rser.2017.03.076.

[19] R. Alayi and H. Rouhi, "Techno-economic analysis of electrical energy generation from urban waste in Hamadan, Iran", *International Journal of Design & Nature and Ecodynamics*, vol. 15, no. 3, pp. 337–341, 2020. DOI: 10.18280/ijdne.150307.

[20] S. K. Kibaara, D. K. Murage, P. Musau, and M. J. Saulo, "Comparative analysis of implementation of solar PV systems using the advanced SPECA modelling tool and HOMER software: Kenyan scenario", *HighTech Innovation Journal*, vol. 1, no. 1, pp. 8–20, 2020. DOI: 10.28991/HIJ-2020-01-01-02.

[21] O. Ayan and B. E. Turkay, "Techno-economic comparative analysis of grid-connected and islanded hybrid renewable energy systems in 7 climate regions, Turkey", *IEEE Access*, vol. 11, pp. 48797–48825, 2023. DOI: 10.1109/ACCESS.2023.3276776.

[22] M. V. Tomovic, D. O. Klimenta, M. J. Milovanovic, B. D. Perovic, and N. L. Hinov, "Optimal design and techno-economic analysis of a hybrid system to supply a remote fishpond with electricity and heat", *Elektronika ir Elektrotechnika*, vol. 30, no. 1, pp. 44–55, 2024. DOI: 10.5755/j02.eie.36123.

[23] E. I. C. Zebra, H. J. van der Windt, G. Nhumaio, and A. P. Faaij, "A review of hybrid renewable energy systems in mini-grids for off-grid electrification in developing countries", *Renewable and Sustainable Energy Reviews*, vol. 144, art. 111036, 2021. DOI: 10.1016/j.rser.2021.111036.

[24] P. H. Kumar, R. R. Gopi, R. Rajarajan, N. B. Vaishali, K. Vasavi, and S. Kumar P, "Prefeasibility techno-economic analysis of hybrid renewable energy system", *e-Prime - Advances in Electrical Engineering, Electronics and Energy*, vol. 7, art. 100443, 2024. DOI: 10.1016/j.prime.2024.100443.

[25] B. K. Das, M. A. Alotaibi, P. Das, M. S. Islam, S. K. Das, and M. A. Hossain, "Feasibility and techno-economic analysis of stand-alone and grid-connected PV/Wind/Diesel/Batt hybrid energy system: A case study", *Energy Strategy Reviews*, vol. 37, art. 100673, 2021. DOI: 10.1016/j.esr.2021.100673.

[26] Z. Li, H. Ye, N. Liao, R. Wang, Y. Qiu, and Y. Wang, "Impact of COVID-19 on electricity energy consumption: A quantitative analysis on electricity", *International Journal of Electrical Power & Energy Systems*, vol. 140, art. 108084, 2022. DOI: 10.1016/j.ijepes.2022.108084.

[27] L. Charfeddine, E. Zaidan, A. Q. Alban, H. Bennasr, and A. Abulibdeh, "Modeling and forecasting electricity consumption amid the COVID-19 pandemic: Machine learning vs. nonlinear econometric time series models", *Sustainable Cities and Society*, vol. 98, art. 104860, 2023. DOI: 10.1016/j.scs.2023.104860.

[28] Z. A. Khan *et al.*, "Modelling electricity consumption during the COVID19 pandemic: Datasets, models, results and a research agenda", *Energy and Buildings*, vol. 294, art. 113204, 2023. DOI: 10.1016/j.enbuild.2023.113204.

[29] "TEİAŞ", 2024. [Online]. Available: https://www.teias.gov.tr/

[30] G.-F. Fan, Y. Zheng, W.-J. Gao, L.-L. Peng, Y.-H. Yeh, and W.-C. Hong, "Forecasting residential electricity consumption using the novel hybrid model", *Energy and Buildings*, vol. 290, art. 113085, 2023. DOI: 10.1016/j.enbuild.2023.113085.

[31] M. Bilgili and E. Pinar, "Gross electricity consumption forecasting using LSTM and SARIMA approaches: A case study of Türkiye", *Energy*, vol. 284, art. 128575, 2023. DOI: 10.1016/j.energy.2023.128575.

[32] A. Yadav and D. K. Vishwakarma, "Sentiment analysis using deep learning architectures: A review", *Artificial Intelligence Review*, vol. 53, no. 6, pp. 4335–4385, 2020. DOI: 10.1007/s10462-019-09794-5.

[33] J. Wu and Y.-G. Wang, "A working likelihood approach to support vector regression with a data-driven insensitivity parameter",

International Journal of Machine Learning and Cybernetics, vol. 14, no. 3, pp. 929–945, 2023. DOI: 10.1007/s13042-022-01672-x.

[34] R. Fu, Z. Zhang, and L. Li, "Using LSTM and GRU neural network methods for traffic flow prediction", in *Proc. of 31st Youth Academic Annual Conference of Chinese Association of Automation*, 2016, pp. 324–328. DOI: 10.1109/YAC.2016.7804912.

[35] S. Selvin, R. Vinayakumar, E. A. Gopalakrishnan, V. K. Menon, and K. P. Soman, "Stock price prediction using LSTM, RNN and CNN-sliding window model", in *Proc. of 2017 International Conference on Advances in Computing, Communications and Informatics*, 2017, pp. 1643–1647. DOI: 10.1109/ICACCI.2017.8126078.

[36] İpekyolu Kalkınma Ajansı, 2019. [Online]. Available: https://www.ika.org.tr/upload/yayinlar/GUNESENERJISI-SEKTOR-RAPORU-759746.pdf